MDPI

Article

A Feasibility Study of CSEM in Geological Advance Forecast with Horizontal Casing Well

Jintai Li [1,2], Jianxin Liu [1,2], Jianqiang Xue [1,2], Rongwen Guo [1,2], Hang Chen [3] and Rong Liu [1,2,*]

1   School of Geosciences and Info-Physics, Central South University, Changsha 410083, China; lijintai2022@126.com (J.L.); ljx6666@126.com (J.L.); yir@mail.xj-n-tax.gov.cn (J.X.); rongwenguo@csu.edu.cn (R.G.)
2   Key Laboratory of Non-Ferrous Resources and Geological Hazard Detection, Central South University, Changsha 410083, China
3   Department of Geosciences, Boise State University, Boise, ID 83725, USA; hangchen@u.boisestate.edu
*   Correspondence: liurongkaoyan@csu.edu.cn

Abstract: With the rapid exploitation of deep mines by digging new tunnels, the advance forecast of water inrush has become increasingly important. The land-based controlled source electromagnetic method (CSEM) is commonly used to detect water-bearing structures. To increase its sensitivity, we propose a new measuring configuration for CSEM by placing EM sensors in an underground steel-cased well. The numerical modeling is conducted by COMSOL to overcome the difficulties of investigating the feasibility of the measuring configuration. The current distribution and electromagnetic field along an in-seam horizontal casing are investigated based on a synthesis three-layered model. The results illustrate that the casing can be treated as antennas that enhance the electric fields at large depths. The water-bearing structures can be observed by a magnetic field (with a perpendicularly horizontal electric dipole (HED) source) rather than an electric field (with a parallelly HED source). Numerical simulations demonstrate that the proposed method is a feasible and effective technique for the detection of water-bearing structures during deep mineral exploration.

Keywords: CSEM; water-bearing structure; horizontal casing well; numerical simulation

1. Introduction

Water inrush is a hazard of shaft mines, especially with the continuous increase of mining depth. The water inrush can lead to mine collapse, resulting in substantial economic losses and casualties [1–3]. The water-bearing structures, often filled with water form age-old goafs, self gobs, small kiln and wasted lane, are major reasons for water inrush accidents [4]. Therefore, it is important to forecast the water-bearing structures to prevent water inrush accidents before tunnel excavation. Because of the low resistivity of the mineralized water, electromagnetic methods have been widely used to the forecast water-bearing structures.

The transient electromagnetic method (TEM) is an efficient tool to detect subsurface objects [5]. Because of its high sensitivity to conductive targets, TEM techniques are commonly used for mapping water-bearing structures above coal seams [6]. However, with the transient loop, the penetration depth of TEM is limited to tens to hundreds of meters [3]. The land-based controlled-source electromagnetic method (CSEM) with a grounded wire source has been applied for targets buried from a few hundred meters to several kilometers. The long-offset TEM (LOTEM) with offsets between 4 and 20 kilometers is suitable for larger detection depths [7,8]. The short-offset TEM (SOTEM) enhances sensitivity by locating the receivers in the near-field region and records the pure secondary field with the EM field excited by a bipolar current [9]. As a classical method, the controlled source audio-frequency magnetotellurics (CSAMT) method, which has been widely applied for the exploration of groundwater, has a high signal-to-noise ratio due to the powerful

transmitter with transmissions up to tens of kilowatts [10]. However, these methods place receivers far away from the low resistivity targets, which results in a low resolution [11]. Typically, the land-based CSEMs are extremely sensitive to shallow surface, which results in difficulties in the extraction of the responses from water-bearing structures [12]. The borehole-to-surface configurations are used for monitoring purposes to enhance the response by hydraulic fracturing in view of the static effect [13].

Currently, the tunnel TEM plays a major role in forecasting water-bearing structures during excavation by moving the devices to the underground roadways of coal mines where they can received stronger responsess from conductive targets [14,15]. Meanwhile, with the development of horizontal well technology, the well-logging-based EM methods have also shown the potential to forecast water-bearing structures [16]. Heagy and Oldenburg examined the response received in iron pipe and compared the influence caused by the static shielding and enhancement effects of iron pipe [17]. Swidinsky and Weiss simulated the response of a coincidence loop in transient induction wireline logging [18]. Tietze et al. investigated the repeatability of land-based CSEM measurements in an active oil field for a vertical well [19]. To obtain strong EM fields with high resolution for water-bear structures, we investigate a CSEM method that uses the grounded wire source of CSAMT and place the receivers inside the horizontal steel casing by numerical modeling.

The steel-cased well can act as a pathway for electric currents at great depths and may enhance resolution for deep targets [20]. However, its extreme geometry (tens of centimeters across, while its length can be kilometers) results a huge mesh of the finite difference method (FDM) and finite element method (FEM) [21]. Furthermore, the system is ill-conditioned for the huge contrast of conductivity between the steel-cased well and the surrounding rocks (the carbon steel has a conductivity of 5.6×10^6 S/m compared to 0.001–1 S/m for the surrounding rocks) [22,23]. Swidinsky et al. used the method of moments (MoM) to calculate the EM signal influenced by steel casings [24]. Kohnke et al. expanded this algorithm to calculate the electromagnetic response of multiple steel-cased wells of arbitrary geometry in a layered model [23]. Although it is a proven effective way to calculate the current distribution along a casing, MoM ignores the interaction between casings and water-bearing structures [25,26]. Fortunately, it has been proven that the COMSOL Multiphysics is a versatile solver for a partial differential equation (PDE) based on a finite elements method [27,28]. The AC/DC module of COMSOL has been widely used for the modeling of electromagnetic problems with steel-cased wells [21,29].

The purpose of this paper is to investigate the feasibility of the CSEM configuration for geological forecast and to study the physics of the electric current affected by a horizontal steel-cased well. Such an arrangement does not appear to have been described before in the geophysical or logging literature. Throughout this very basic study, we investigate the electromagnetic field along the horizontal steel-cased well with the parallelly and perpendicularly grounded horizontal electric dipole (HED) source, respectively. The application program interface(API) of the AC/DC module in COMSOL is applied with Matlab to carry out the numerical simulation of synthetic models with steel casings. The results illustrate that this measuring configuration is effective and accurate.

2. Materials and Methods

The Magnetic Fields interface in the AC/DC module of COMSOL-linked Matlab (version 5.6, Comsol AB, Stockholm, Sweden) is employed for numerical simulations in the frequency domain. The Maxwell equation is solved using certain boundary condition as:

$$(j\omega\sigma - \omega^2\epsilon_0\epsilon_r)\boldsymbol{A} + \nabla \times \boldsymbol{H} = \boldsymbol{J_e}, \tag{1}$$

where $\boldsymbol{H}$ is the magnetic field. Note that $\boldsymbol{H}$ and $\boldsymbol{B}$, the magnetic flux density, are related by $\mu_0\mu_r\boldsymbol{H} = \boldsymbol{B}$, where μ_0 is the magnetic permeability of free space and μ_r (=1) is the relative permeability. Here, $j = \sqrt{-1}$ is the pure imaginary number which is a dimensionless number, and ω is the angular frequency (in rad/s). σ is the conductivity (in S/m) which is treated as a real number by neglecting polarization. ϵ_0 and ϵ_r (=1) are the electric

permittivity of free space (in $C^2/(N \cdot M^2)$) and the relative permittivity of the medium, respectively. A is the magnetic vector potential (in T·m). Once A is solved, the magnetic flux density can be obtained by $B = \nabla \times A$. J_e is the external current density (in A/m^2).

To solve Equation (1), boundary conditions should be included. In the functionality of the Magnetic Fields interface, the magnetic insulation boundary condition, which is also known as the Dirichlet boundary condition, is used. On the outer boundary of the model domain, it is defined as:

$$\hat{n} \times A_{\Gamma} = 0, \tag{2}$$

where Γ is the outer boundary of the model domain, and $\hat{n}$ is the normal vector of the outer boundary.

Meanwhile, it is necessary to determine the size of the simulation domain. Typically, once the Dirichlet boundary condition is used, the outer boundary should be with a distance larger than several times the detection depth away from the region of interest to keep the accuracy [30]. Here, the detection depth is estimated by the skin depth (assumed as δ in this paper), which is defined by $\delta = \sqrt{2/\omega\mu_0\sigma}$. The infinity element domain is applied to stretch the finite elements in the radial direction so that the outer boundary conditions can be sufficiently satisfied [27,31].

The Impedance Transition Boundary Condition (ITBC) is used to model a highly conductive steel-cased well [32,33]. It can effectively simulate the high conductivity characteristics of the casing (indicated in Figure 1).
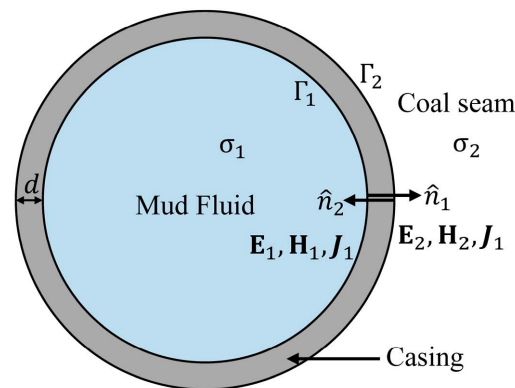

Figure 1. Cross section of the thin conductive casing.

By introducing transfer and surface impedances, the current density and the tangential electric field on both sides of the casing surface can be related as:

$$J_{s1} = \frac{Z_s E_{t1} - Z_t E_{t2}}{Z_s^2 - Z_t^2}, \tag{3}$$

$$J_{s2} = \frac{Z_s E_{t2} - Z_t E_{t1}}{Z_s^2 - Z_t^2}, \tag{4}$$

where J_{s1} and J_{s2} are the the current flowing on both sides of the casing surface, while E_{t1} and E_{t2} are the the tangential electric field. Z_t and Z_s are the transfer and surface impedances, which can be evaluated by:

$$Z_t = \frac{-j\omega\mu_0\mu_r}{k} \frac{1}{tan(kd)}, \tag{5}$$

$$Z_s = \frac{-j\omega\mu_0\mu_r}{k} \frac{1}{sin(kd)}, \tag{6}$$

where d is the thicknss of the steel-cased well (in m), and k is the wave number, which is defined by $k = \omega\sqrt{\epsilon_0\epsilon_r + \mu_0\mu_r(\sigma/(j\omega))}$. ITBC significantly reduces the numbers of grid cells and satisfies the discontinuity of the electric field at the casing interface [34,35]. The relationship between current density and the magnetic field on both surfaces of the casing can be described by:

$$\hat{n}_1 \times \boldsymbol{H}_1 = \boldsymbol{J}_{s1}, \tag{7}$$

$$\hat{n}_2 \times \boldsymbol{H}_2 = \boldsymbol{J}_{s2}, \tag{8}$$

where $\hat{n}$ is the normal vector, and $\boldsymbol{H}_1$ and $\boldsymbol{H}_2$ are the magnetic field on the two side surfaces of the casing. By eliminating $\boldsymbol{J}$, (3), (4), (7) and (8) can usually be rewritten in a matrix as:

$$\begin{bmatrix} \hat{n}_1 \times \boldsymbol{H}_1 \\ \hat{n}_2 \times \boldsymbol{H}_2 \end{bmatrix} = \begin{bmatrix} Y_{11} & Y_{12} \\ Y_{21} & Y_{22} \end{bmatrix} \begin{bmatrix} \hat{n}_1 \times \hat{n}_1 \times \boldsymbol{E}_1 \\ \hat{n}_2 \times \hat{n}_2 \times \boldsymbol{E}_2 \end{bmatrix}, \tag{9}$$

where

$$Y_{11} = Y_{22} = \frac{Z_t}{Z_t^2 - Z_s^2}, \tag{10}$$

$$Y_{12} = Y_{21} = -\frac{Z_s}{Z_t^2 - Z_s^2}, \tag{11}$$

Once we have handled all the parameters of the mesh, a solver should be selected to solve the system. As the matrix of electromagnetic problem is ill-conditioned, the direct solver is preferred rather than the iterative solver. Although a direct solver will be memory demanding, it is generally accepted to be much more robust than iterative ones [31,36]. A MUMPS (Multifrontal Massively Parallel Sparse) direct solver is used for all the numerical simulations in this paper [37].

3. Results

In this section, we first consider a model with two vertical steel-cased wells to validate the finite element results in COMSOL Multiphysics with the analytical solution from Patzer et al. [21]. Then, in Sections 3.2 and 3.3, the performance of the CSEM configurations with a grounded HED source (which is either parallel or perpendicular to the horizontal part of an 'L' shape casing) are examined, respectively. More specifically, a typical three-layer model with a horizontal steel-cased well is designed to examine the potential of our proposed configurations by numerical modeling using COMSOL. A quite fine mesh is employed inside the wells to ensure the accuracy of the electromagnetic field. The direct solver MUMPS is used to solve the linear equations with a larger condition number. These programs were run on a personal computer with 32G RAM, 3.6GHz and 8 cores.

3.1. Numerical Verification

To verify the validity of our work, two vertical steel-cased wells were placed 50 m and 500 m away from a 1000 m length grounded HED source, as shown in Figure 2a. The steel-cased wells were approximated with high conductivity solid cylinders with a radius of 1 m and a length of 1000 m. The conductivity of both steel-cased wells were 5×10^4 S/m, and the conductivity of the homogeneous half-space was 0.3333 S/m. The relative current strength along the two steel-cased wells was measured with a source frequency of 1 Hz. As shown in Figure 2b, the solution of COMSOL (the solid lines) agrees well with the analytical solution (the dashed lines) of Patzer et al. [21]. The results indicated that the partial differential equation solver in COMSOL's API can provide accurate results for the problem with high conductivity and complex geometry wells .
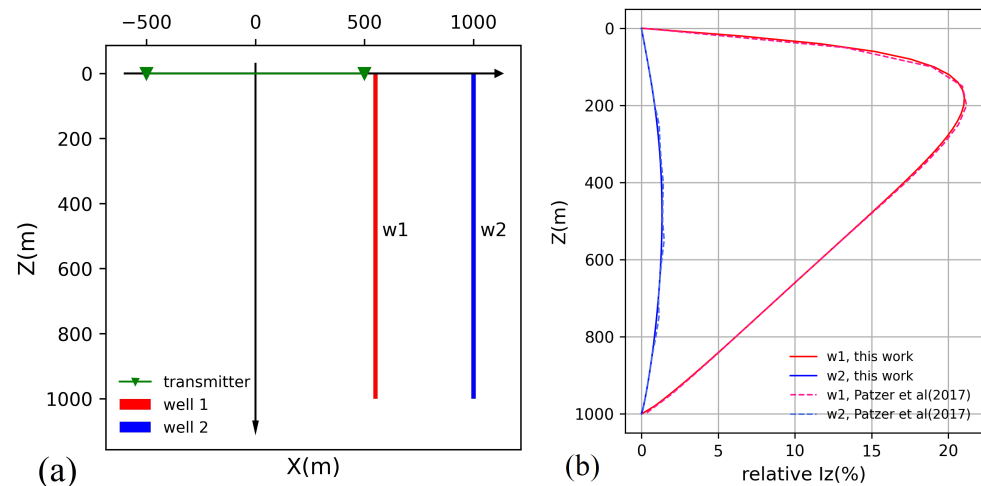
Figure 2. (**a**) A model with two vertical steel-cased wells. The wells w1 (red solid line) and w2 (blue solid line) are placed 50 and 500 m away from the 1000 m length grounded HED source (green solid line), respectively. The wells are assumed as solid cylinders with a 1 m radius and a 1000 m length which have a conductivity of 5×10^4 S/m. (**b**) The relative current strength along two wells, which are normalized by the transmitter. The results of this work and the analytical solution in Patzer et al. are indicated by solid lines and dashed lines, respectively [21].

3.2. The x-Component of the Electric Field with a Parallelly Grounded HED

With a parallelly grounded HED source, we designed a typical three-layer model, indicated in Figure 3, to simulate the EM field measured along the horizontal casing. A thin layer of 0.005 S/m with a 20 m thickness (represents the coal seam) is embedded in a 0.01 S/m homogenous half space at a depth of 300 m. An 'L' shape casing with a uniform outer diameter (0.2 m) and thickness (0.005 m) and a conductivity of 5.6×10^6 S/m is embedded in the model at a depth of 310 m, whose vertical and horizontal parts with lengths of 310 m and 1000 m, respectively. The horizontal casing along the coal seam was filled with a mud fluid of conductivity of 10 S/m. Within the Cartesian coordinate system, the center of the x-directed horizontal casing located at (0, 0, −310) m. An x-directed grounded HED source with its center located at (0, −2000, 0) m was 2000 m away from the horizontal casing along the y-axis to alleviate the near field effects. The HED source was a 1000 m long wire carrying a 10 A alternating current. The frequency of 32 Hz was believed appropriate for our test purposes based on the skin-depth calculation [38]. To illustrate the electromagnetic field along the horizontal casing by the water-bearing structure at different positions, four water-bearing structures were considered, respectively. Each of these water-bearing structures was approximated by a conductive cube with a conductivity of 1 S/m and had a dimension of $20 \times 20 \times 20$ m^3. As shown in Figure 3, these cubes were represented by A, B, C and D.
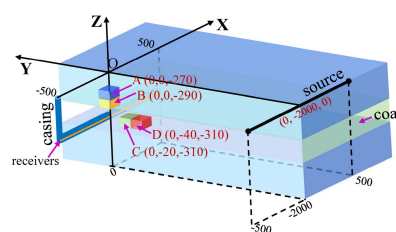

Figure 3. Measurement configuration for a grounded HED parallel to a horizontal casing. The 'L' shape casing consists of a 310 m long vertical part and a 1000 m long horizontal part. The HED source is 1000 m long carrying a 10 A current at a frequency of 32 Hz. Four different water-bearing structures, represented by A (at (0, 0, −270) m), B (at (0, 0, −290) m), C (at (0, −20, −310) m) and D (at (0, −40, −310) m), are considered separately.

Figure 4a shows the amplitude difference of the x-component electric field inside the horizontal casing caused by each cube normalized by the background field (the model consists of three-layered earth and casing). Figure 4b shows the relative difference of the corresponding phase difference. The cube B and C closer to the casing than cubes A and D lead to a larger difference. However, there is no significant disturbance caused by the cubes. Note that with the parallelly source, the H_x along the horizontal casing tends to zero and is not presented. With a maximum relative difference smaller than 0.1%, the surrounding water-bearing structures of coal seams are unobservable for a parallelly grounded HED configuration.


(a)

(b)
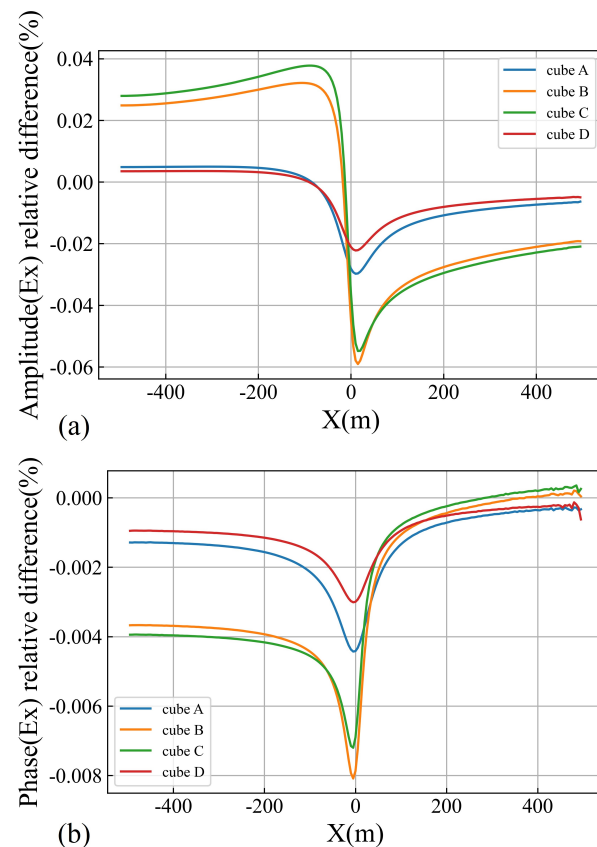
Figure 4. (**a**) Amplitude relative difference of the electric field along the horizontal casing for each cube, normalized by the background field; (**b**) Phase relative difference of the electric field along the horizontal casing for each cube, normalized by the background field.

Figure 5 aims to show how the steel-cased well and the anisotropy of the coal seam influence the electric field along the casing. In such cases, no cube is considered, and the conductivity of the coal seam in a vertical direction (=0.0005 S/m) is assumed as one-tenth of that in a horizontal direction (=0.005 S/m). The green curve and the red curve in Figure 5a, which almost overlap, show that anisotropy of the coal seam has little effect on the field. The consistency of these curves along the horizontal casing implies vertical incidence of the EM wave. Both green and red curves show much higher amplitude than that of curves with the casing. The amplitude of the electric field inside the horizontal casing is weakened due to the shielding effect of the steel-cased well. The asymmetric form of the blue and orange curves in both Figure 5a,b indicates that the vertical steel-cased well redistributes the current which is agreed with the research from [20]. Meanwhile, Figure 5a,b demonstrate that the anisotropy of the coal seam is negligible with a parallelly HED source, while the casing significantly affects the electric field along the horizontal casing.

(a)

(b)
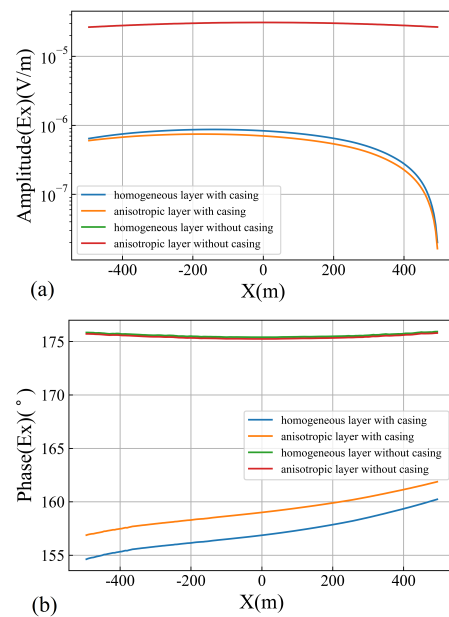
Figure 5. (**a**) Amplitude of the electric field along the horizontal casing to show the effect of the anisotropy and casing; (**b**) Phase of the electric field along the horizontal casing to show the effect of the anisotropy and casing.

To better illustrate the effect of the steel-cased well on the current distribution, we visualized the underground current distribution of the layer model in Figure 6. Figure 6a shows the current distribution (represented as log base 10) at the section view at y = 0 m of the layer model in Figure 3 with the casing, while Figure 6b shows the current distribution without the casing. The contrast between Figure 6a,b demonstrates that both the vertical casing and the horizontal casing result in increasing the current underground, which agrees with the results by Commer et al. [20].

(a)

(b)
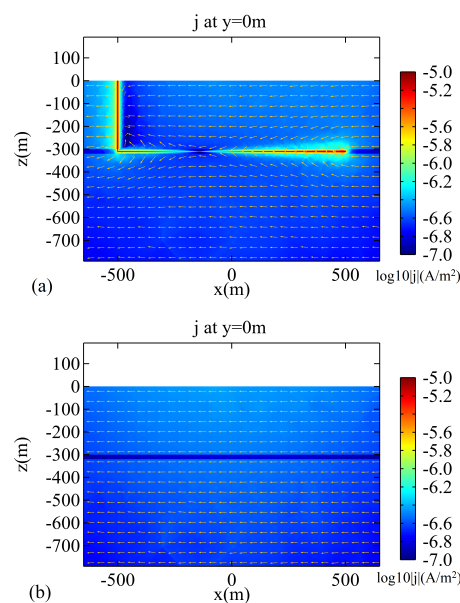
Figure 6. The current distribution (represented as log base 10) at a section view at y=0 m of the layer model in Figure 3: (**a**) current distribution with casing; (**b**) current distribution without casing.

Figure 7 shows the x-component and z-component of the current distribution at a section view at y = 0 m. Figure 7a,b demonstrate that the steel-cased well mainly strengthens the normal current. The 'L' shape steel-cased well is acting as a dipole source. As shown

in Figures 6 and 7, the current transports from the left with an x-coordinate less than −100 m to the right part of the casing in the half space. Note that the steel-cased well is just a hypothetical electric dipole, which does not provide any extra current to the underground space.

(a)

(b)
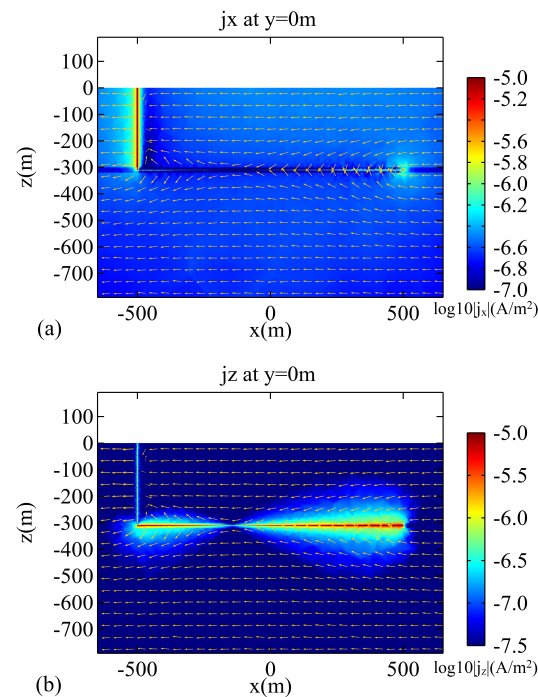
Figure 7. (**a**) The x-component current distribution (represented as log base 10) at a section view at y = 0 m of the layer model in Figure 3; (**b**) The z-component current distribution (represented as log base 10) at a section view at y = 0 m of the layer model in Figure 3.

3.3. The x-Component of the Magnetic Field with a Perpendicularly HED

Figure 8 shows the model to investigate the magnetic field along the horizontal casing with a perpendicularly HED source. The geometry and electric parameters of a three-layered model, an 'L' shape casing model and four cubes are consistent with Section 3.2. The center and orientation of the grounded HED source is different from the previous work in Section 3.2. The grounded HED source is carrying alternative 10 A current at 128 Hz, with its center located at (2000, 0, 0) m is perpendicular to the horizontal casing.
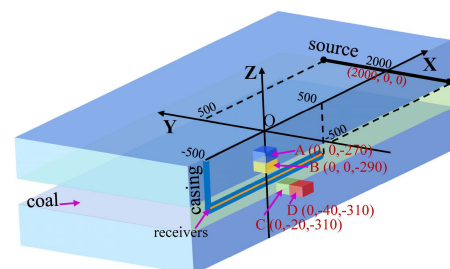
Figure 8. Measurement configuration for a grounded HED perpendicular to a horizontal casing. The 'L' shape casing consists of a 310 m long vertical part and a 1000 m long horizontal part. The HED source is 1000 m long carrying 10 A current at a frequency of 128 Hz. Four different water-bearing structures, represented by A (at (0, 0, −270) m), B (at (0, 0, −290) m), C (at (0, −20, −310) m) and D (at (0, −40, −310) m), are considered, respectively.

Figure 9a shows the amplitude difference of the x-component magnetic field inside the horizontal casing caused by each conductive cube normalized by the background field (the

model consists of three-layered earth and casing), and Figure 9b shows the corresponding phase difference. The magnetic field relative difference along the horizontal casing caused by the conductive body above the casing (cube A and B) approaches 2%. Although the presence of casing underground distorts the electromagnetic field, it is concluded that a relative variation of electromagnetic field above 1% can be considered as a signal from the anomalous body underground [38,39].
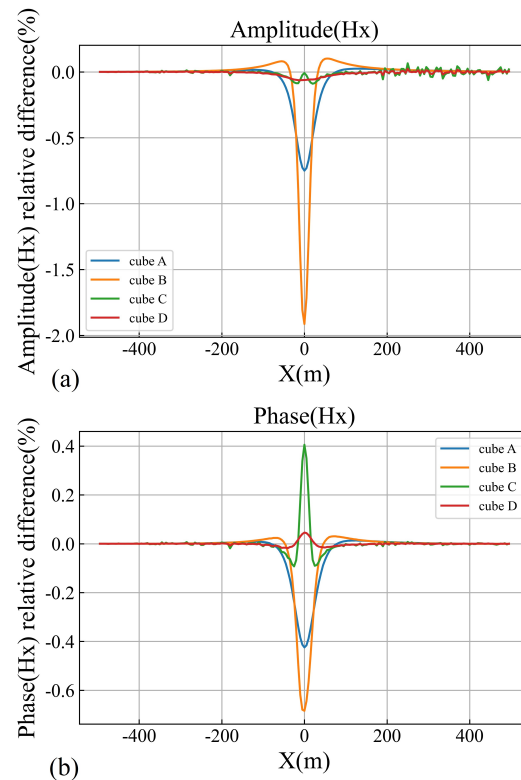

Figure 9. (**a**) Amplitude relative difference of the magnetic field along the horizontal casing for each cube, normalized by the background field; (**b**) Phase relative difference of the magnetic field along the horizontal casing for each cube, normalized by the background field.

Figure 10 shows the influence of the anisotropy of the coal seam and the casing on the H_x component signal. Different from the significant influence on the E_x component response for a parallelly HED source shown in Figure 5, the existence of casing has little effect on the H_x component for a perpendicularly HED source. Note that with the perpendicularly source, the electric field along the horizontal casing tends to zero and is not presented. Figure 10 demonstrates that the casing is negligible with a perpendicularly HED source, while the anisotropy of the coal seam significantly affects the magnetic field along the horizontal casing.

These two numerical experiments on the synthetic model for the transmitter parallel and perpendicular to the horizontal casing are applied to assess the effect of casing and the feasibility of our proposed configuration. Due to the shielding effect, the steel-cased well can result in a significant difference to the electric field along the horizontal casing for the case with a parallelly grounded HED source. The electric field in the casing has a relative difference below 0.1% to the background field. The above features demonstrate that a measuring configuration with the parallel HED source is ineffective for detecting water-bearing structures in a geological forecast.

On the contrary, the shielding effect of the casing has little effect on the magnetic field along the horizontal casing with a perpendicularly grounded HED source, and the relative difference caused by the conductive cube approaches 2%. A magnetic field measure-

ment configuration with perpendicular HED has the potential of detecting water-bearing structures in geological forecasting.
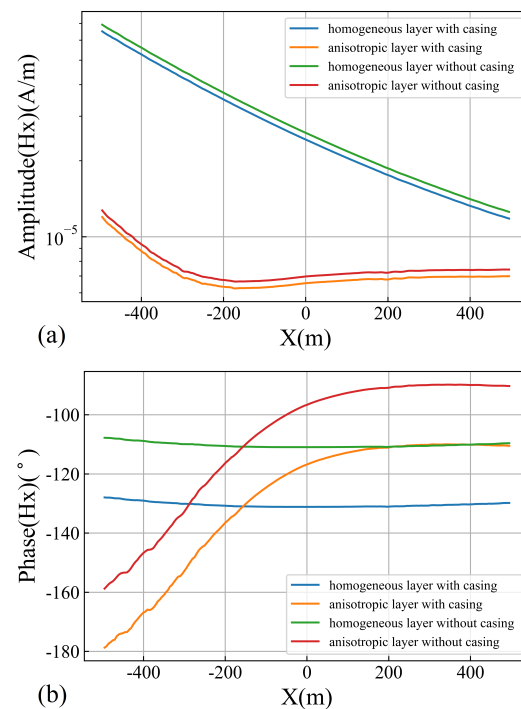
Figure 10. (**a**) Amplitude of the magnetic field along the horizontal casing to show the effect of the anisotropy and casing; (**b**) Phase of the electric field along the horizontal casing to show the effect of the anisotropy and casing.

4. Conclusions

We proposed a measuring framework of a CSEM method by placing EM sensors along a horizontal casing well. The commonly grounded HED source by CSAMT was employed as the transmitter which was either parallel or perpendicular to the horizontal casing. A typical three-layered model with a conductive prism around the horizontal casing well was designed to represent a water-bearing structure in coal mines. The numerical modeling by employing the COMSOL was carried out to get the EM response of water-bearing structures near the horizontal casing. The numerical solution was verified by the analytical solution on a model with two steel casings. The distribution of electric current showed that the steel-cased well embedded in the coal seams acted as a dipole in the earth, which is consistent with previous research. The electric field along the horizontal casing well (with a parallelly grounded HED) had amplitudes larger than 1×10^{-7} V/m, and the water-bearing structure will result in a relative difference of 0.06%. With a perpendicularly grounded HED source, the shielding effect of the steel casing can be ignored. The magnetic field along the horizontal casing well (with a perpendicularly grounded HED) had amplitudes larger than 1×10^{-5} A/m, and the water-bearing structure will result in a relative difference up to 2%. Although a relative difference of 5% is widely accepted by land-based CSEM, we take an optimistic view on our proposed method since the EM field in the horizontal casing suffers less from surface noise.

Author Contributions: Conceptualization, R.G. and R.L.; methodology, J.L. (Jintai Li); software, H.C.; validation, H.C. and J.L. (Jintai Li); formal analysis, J.L. (Jintai Li); investigation, R.L.; resources, H.C. and J.X.; data curation, J.L. (Jintai Li) and H.C.; writing—original draft preparation, J.L. (Jintai Li); writing—review and editing, R.L. and J.X.; visualization, J.L. (Jintai Li) and H.C.; supervision, J.L. (Jianxin Liu); project administration, R.G.; funding acquisition, J.L. (Jianxin Liu). All authors have read and agreed to the published version of the manuscript.

Conflicts of Interest: The authors declare no conflict of interest.

References

1. Zhang, J.; Shen, B. Coal mining under aquifers in China: A case study. *Int. J. Rock Mech. Min. Sci.* **2004**, *41*, 629–639. [CrossRef]
2. Yao, B.; Wei, J.; Wang, D.; Ma, D.; Chen, Z. Numerical study on seepage property of karst collapse columns under particle migration. *Comput. Model. Eng. Sci.* **2013**, *91*, 81–100. [CrossRef]
3. Chen, W.Y.; Xue, G.Q.; Muhammad, Y.K.; Gelius, L.J.; Zhou, N.N.; Li, H.; Zhong, H.S. Application of Short-Offset TEM (SOTEM) Technique in Mapping Water-Enriched Zones of Coal Stratum, an Example from East China. *Pure Appl. Geophys.* **2015**, *172*, 1643–1651. [CrossRef]
4. Xu, C.; Gong, P. Water Disaster Types and Water Control Measures of Hanxing Coal Mine Area. *Procedia Earth Planet. Sci.* **2011**, *3*, 343–348. [CrossRef]
5. Chen, W.; Xue, G.; Olatayo, A.L.; Chen, K.; Younis Khan, M.; Chen, W.; Zhang, L.; Chen, W. A comparison of loop time-domain electromagnetic and short-offset transient electromagnetic methods for mapping water-enriched zones—A case history in Shaanxi, China. *Geophysics* **2017**, *82*, B201–B208. [CrossRef]
6. Liu, Y.; Yin, C.; Qiu, C.; Hui, Z.; Zhang, B.; Ren, X.; Weng, A. 3-D inversion of transient EM data with topography using unstructured tetrahedral grids. *Geophys. J. Int.* **2019**, *217*, 301–318. [CrossRef]
7. Newman, G.A. Deep transient electromagnetic soundings with a grounded source over near-surface conductors. *Geophys. J. Int.* **1989**, *98*, 587–601. [CrossRef]
8. Caldwell, T.G.; Bibby, H.M. The instantaneous apparent resistivity tensor: A visualization scheme for LOTEM electric field measurements. *Geophys. J. Int.* **1998**, *135*, 817–834. [CrossRef]
9. Xue, G.Q.; Chen, W.Y.; Zhou, N.N.; Li, H. Short-offset TEM technique with a grounded wire source for deep sounding. *Chin. J. Geophys.* **2013**, *56*, 255–261. [CrossRef]
10. Fu, C.; Di, Q.; An, Z. Application of the CSAMT method to groundwater exploration in a metropolitan environment. *Geophysics* **2013**, *78*, B201–B209. [CrossRef]
11. Jiang, Z.; Liu, L.; Liu, S.; Yue, J. Surface-to-Underground Transient Electromagnetic Detection of Water-Bearing Goaves. *IEEE Trans. Geosci. Remote Sens.* **2019**, *57*, 5303–5318. [CrossRef]
12. Streich, R.; Becken, M. Sensitivity of controlled-source electromagnetic fields in planarly layered media: CSEM sensitivity in VTI-anisotropic media. *Geophys. J. Int.* **2011**, *187*, 705–728. [CrossRef]
13. Streich, R. Controlled-Source Electromagnetic Approaches for Hydrocarbon Exploration and Monitoring on Land. *Surv. Geophys.* **2016**, *37*, 47–80. [CrossRef]
14. Jiang, Z.; Liu, S.; Malekian, R. Analysis of a Whole-Space Transient Electromagnetic Field in 2.5-Dimensional FDTD Geoelectric Modeling. *IEEE Access* **2017**, *5*, 18707–18714. [CrossRef]
15. Jiang, Z.H.; Yue, J.H.; Liu, S.C. Prediction Technology of Buried Water-Bearing Structures in Coal Mines Using Transient Electromagnetic Method. *J. China Univ. Min. Technol.* **2007**, *17*, 164–167. [CrossRef]
16. Zhang, Z.; Xiao, J. Inversions of surface and borehole data from large-loop transient electromagnetic system over a 1-D earth. *Geophysics* **2001**, *66*, 1090–1096. [CrossRef]
17. Heagy, L.J.; Oldenburg, D.W. Modeling electromagnetics on cylindrical meshes with applications to steel-cased wells. *Comput. Geosci.* **2019**, *125*, 115–130. [CrossRef]
18. Swidinsky, A.; Weiss, C.J. On coincident loop transient electromagnetic induction logging. *Geophysics* **2017**, *82*, E211–E220. [CrossRef]
19. Tietze, K.; Ritter, O.; Patzer, C.; Veeken, P.; Dillen, M. Repeatability of land-based controlled-source electromagnetic measurements in industrialized areas and including vertical electric fields. *Geophys. J. Int.* **2019**, *218*, 1552–1571. [CrossRef]
20. Commer, M.; Hoversten, G.M.; Um, E.S. Transient-electromagnetic finite-difference time-domain earth modeling over steel infrastructure. *Geophysics* **2015**, *80*, E147–E162. [CrossRef]
21. Patzer, C.; Tietze, K.; Ritter, O. Steel-cased wells in 3-D controlled source EM modelling. *Geophys. J. Int.* **2017**, *209*, 813–826. [CrossRef]
22. Frischknecht, F.C. 6. Electromagnetic Physical Scale Modeling. In *Electromagnetic Methods in Applied Geophysics: Volume 1, Theory*; Investigations in Geophysics, Society of Exploration Geophysicists: Houston, TX, USA, 1988; pp. 364–441. [CrossRef]
23. Kohnke, C.; Liu, L.; Streich, R.; Swidinsky, A. A method of moments approach to model the electromagnetic response of multiple steel casings in a layered earth. *Geophysics* **2018**, *83*, WB81–WB96. [CrossRef]
24. Swidinsky, A.; Edwards, R.N.; Jegen, M. The marine controlled source electromagnetic response of a steel borehole casing: Applications for the NEPTUNE Canada gas hydrate observatory. *Geophys. Prospect.* **2013**, *61*, 842–856. [CrossRef]

25. Yang, W.; Torres-Verdín, C.; Hou, J.; Zhang, Z.I. 1D subsurface electromagnetic fields excited by energized steel casing. *Geophysics* **2009**, *74*, E159–E180. [CrossRef]

26. Schamper, C.; Rejiba, F.; Tabbagh, A.; Spitz, S. Theoretical analysis of long offset time-lapse frequency domain controlled source electromagnetic signals using the method of moments: Application to the monitoring of a land oil reservoir. *J. Geophys. Res. Solid Earth* **2011**, *116*. [CrossRef]

27. Multiphysics, C. *COMSOL Multiphysics User's Guide*; Version 5.6; Comsol AB: Stockholm, Sweden, 2021.

28. Chen, H.; Niu, Q. Effects of material texture and packing density on the interfacial polarization of granular soils. *Geophysics* **2021**, *86*, MR285–MR297. [CrossRef]

29. Orujov, G.; Anderson, E.; Streich, R.; Swidinsky, A. On the electromagnetic response of complex pipeline infrastructure. *Geophysics* **2020**, *85*, E241–E251. [CrossRef]

30. Butler, S.L.; Zhang, Z. Forward modeling of geophysical electromagnetic methods using Comsol. *Comput. Geosci.* **2016**, *87*, 1–10. [CrossRef]

31. Qi, Y.; El-Kaliouby, H.; Revil, A.; Soueid Ahmed, A.; Ghorbani, A.; Li, J. Three-dimensional modeling of frequency- and time-domain electromagnetic methods with induced polarization effects. *Comput. Geosci.* **2019**, *124*, 85–92. [CrossRef]

32. Horton, R.; Easter, B.; Gopinath, A. Variation of microstrip losses with thickness of strip. *Electron. Lett.* **1971**, *7*, 490–491. [CrossRef]

33. Sun, Q.; Zhang, R.; Zhan, Q.; Liu, Q.H. Multiscale Hydraulic Fracture Modeling With Discontinuous Galerkin Frequency-Domain Method and Impedance Transition Boundary Condition. *IEEE Trans. Geosci. Remote Sens.* **2017**, *55*, 6566–6573. [CrossRef]

34. Van den Berghe, S.; Olyslager, F.; De Zutter, D. Accurate modeling of thin conducting layers in FDTD. *IEEE Microw. Guid. Wave Lett.* **1998**, *8*, 75–77. [CrossRef]

35. Woyna, I.; Gjonaj, E.; Weiland, T. Broadband surface impedance boundary conditions for higher order time domain discontinuous Galerkin method. *COMPEL: Int. J. Comput. Math. Electr. Electron. Eng.* **2014**, *33*, 1082–1096. [CrossRef]

36. Cai, H.; Hu, X.; Li, J.; Endo, M.; Xiong, B. Parallelized 3D CSEM modeling using edge-based finite element with total field formulation and unstructured mesh. *Comput. Geosci.* **2017**, *99*, 125–134. [CrossRef]

37. Amestoy, P.R.; Duff, I.S.; L'Excellent, J.Y. Multifrontal parallel distributed symmetric and unsymmetric solvers. *Comput. Methods Appl. Mech. Eng.* **2000**, *184*, 501–520. [CrossRef]

38. Liu, R.; Liu, J.; Wang, J.; Liu, Z.; Guo, R. A time-lapse CSEM monitoring study for hydraulic fracturing in shale gas reservoir. *Mar. Pet. Geol.* **2020**, *120*, 104545. [CrossRef]

39. Wirianto, M.; Mulder, W.; Slob, E. A feasibility study of land CSEM reservoir monitoring in a complex 3-D model. *Geophys. J. Int.* **2010**, *181*, 741–755. [CrossRef]